System Design and Experimental Demonstration of Spherical Piezoelectric Ceramic Transformers in Radial Vibration

Yifan Tang and Shuyu Lin

***Abstract*—As a prevalent type of transformer, piezoelectric transformers have garnered significant attention in various practical applications due to their lighter, smaller construction and absence of magnetic fields. Recent advances in the field of piezoelectric transformers have developed a variety of structure types, while the piezoelectric transformer with a spherical shape has not been researched. Here, we present a spherical piezoelectric ceramic transformer capable of achieving both step-up and step-down output characteristics in radial vibration. The resulting design is made of two layers of piezoceramic spherical shells and three layers of metal spherical shells. The basic mechanism is that the input electrical energy is converted into mechanical energy via the inverse piezoelectric effect, and then the converted mechanical energy is reconverted into electrical energy, thus realizing step-up and step-down voltage conversions. The electromechanical characteristics, voltage gain, and power gain for our proposed spherical piezoceramic transformer as functions of electric load resistance and geometry size under different dielectric and mechanical losses are analyzed. The experiments are conducted to verify the performance parameters of our proposed design, which are basically consistent with the results of numerical simulation and theoretical analysis. The power gain of our proposed spherical piezoceramic transformer can reach about 36% when the input voltage of the function generator is 20 V peak-to-peak and the load resistance is 125 Ω. The resonance frequency of the spherical piezoelectric transformer can be varied from 75 839 to 74 221 Hz by varying the thickness of the intermediate metal spherical shell from 0.2 to 3.8 mm. Our methodology will open new perspectives for the design of piezoelectric transformers, which may have prominent applications in various fields, such as portable electronic chargers and electronic ballasts for fluorescent lamps.**

***Index Terms*—Piezoelectric transformer, power gain, radial vibration, spherical transducers.**

I. Introduction

With the rapidly developing electronic technology, a great number of electrical devices require step-up or step-down source voltage to meet their needs [1], [2], [3], [4], [5]. Over the past few decades, a major advance has been made in the research of piezoelectric transformers, which can be used to convert primary voltages into proportional voltages in the secondary by utilizing the inverse piezoelectric effect and the piezoelectric effect. Therefore, piezoelectric transformers have been extensively utilized in various application scenarios, such as electronic ballasts for fluorescent lamps, electrostatic copiers, small power laser tube power supplies, and dc/dc converters [6], [7], [8], [9]. Unlike conventional electromagnetic transformers [10], piezoelectric transformers feature a small size, a simple structure, high conversion efficiency, and easy mass production [11], [12], [13], [14], [15], [16]. Moreover, piezoelectric transformers produce very little electromagnetic interference and are less likely to burn than winding-type components, so they are safer. Rosen first proposed the Rosen-type piezoelectric transformer, which is composed of a piezoelectric actuator in transverse vibration mode and a piezoelectric transducer in longitudinal vibration mode [17]. Zaitsu et al. [18] presented the thickness vibration mode piezoelectric transformer and derived its equivalent circuit model, which is made of a piezoelectric actuator and a piezoelectric transducer both in longitudinal vibration mode. Baker et al. [19] demonstrated a piezoelectric transformer in radial vibration used in fluorescent ballast applications, and the design program was validated with a custom-designed piezoelectric transformer running in a 32 W ballast. The shear vibration mode piezoelectric transformer varies from the three transformers mentioned above in that the direction of the electric field applied by the driving section is perpendicular to the direction of polarization, while the electric field generated by the generating section is parallel to the direction of polarization. The excitation at the primary generates shear stresses inside the transformer, which in turn generates voltage in the secondary [20]. To increase the step-down or step-up voltage conversion, the piezoelectric transducer or piezoelectric actuator may consist of multiple layers of piezoelectric material, which is called a multilayer piezoelectric transformer [21], [22], [23], [24]. Recently, Lin et al. [25] reported and fabricated a novel wireless power transmission system, which consists of two sandwiched composite piezoelectric transducers connected in the center by a metallic transmission cylinder. Subsequently, Lin et al. proposed two new radially vibrating ring-type piezoelectric ceramic transformers. One consists of two concentric piezoceramic rings with axial and radial polarization, and the other is composed of a

Received 11 December 2024; revised 31 March 2025 and 8 July 2025; accepted 24 July 2025. Date of publication 4 August 2025; date of current version 8 September 2025. This work was supported in part by the National Natural Science Foundation of China under Grant 12174240 and Grant 12404532 and in part by the Fundamental Research Funds for the Central Universities under Grant 020414380195 and Grant GK202506011. Recommended for publication by Associate Editor G.-S. Seo. *(Corresponding author: Shuyu Lin.)*

The authors are with the Shaanxi Key Laboratory of Ultrasonics, Institute of Applied Acoustics, Shaanxi Normal University, Xian 710119, China (e-mail: tangyifan@snnu.edu.cn; sylin@snnu.edu.cn).

Color versions of one or more figures in this article are available at https://doi.org/10.1109/TPEL.2025.3593814.

Digital Object Identifier 10.1109/TPEL.2025.3593814

TABLE I
MAIN TYPES OF PIEZOELECTRIC CERAMIC TRANSFORMERS

Type	Structural Features	Applications	Advantages	Disadvantages
Rosen type	Elongated ceramic strip, vibration node at the center.	High-voltage power supplies, LCD backlights	High voltage gain (up to kV), efficiency >90%	Large size, low operating frequency (kHz range)
Thickness vibration mode	Compact construction, high frequency operation	Miniaturized devices, wireless energy transfer systems	Small size, high-frequency compatibility, suitable for thin-film integration	Limited power capacity, poor heat dissipation
Radial vibration mode	Disc/ring structure, upper and lower surface electrodes	Medium-voltage conversion, ultrasonic generators	Simple structure, adaptable to mid-low voltage	Limited power output, narrow frequency bandwidth
Multilayer stack	Multiple ceramic layers, enhances power density	High-power industrial equipment, energy harvesting	High power density, flexible voltage output, strong insulation	Complex design, susceptible to delamination failure
Radial vibration mode	Spherical shell structure	Portable electronic chargers	Step-up and step-down output	Require high manufacturing precision

pair of concentric piezoceramic circular disk and ring [26], [27]. Wang et al. proposed a piezoceramic transformer on the basis of the sandwiched piezoelectric transducer having multiple output properties. The output power for the piezoelectric transformer can reach 45 W while simultaneously maintaining an efficiency of ∼35% [28]. The main types of piezoelectric ceramic transformers are illustrated in Table I. Recent advances in piezoelectric spherical transducers have improved the electromechanical performance and application range of spherical transducers [29], [30], [31], [32], and a large number of piezoelectric transformers with different vibration modes and shapes have been proposed. However, the spherical piezoelectric ceramic transformer (SPCT) in radial vibration has not been researched. Given the complexity of real-world problems, some significant scenarios may require the SPCT to achieve step-up and step-down outputs, such as portable electronic chargers, battery chargers for mobile phones, and several other relevant underlying applications. It is of great practical significance to investigate the variation of the voltage and power gains and electromechanical properties with the geometrical dimensions and electric load resistance under different dielectric and mechanical losses.

In this work, we report an SPCT capable of realizing step-up and step-down output characteristics. Our device consists of three concentric spherical metal shells and two radially polarized spherical piezoelectric ceramic shells. By introducing metal spherical shells, the mechanical strength of the transformer can be increased. The distributed parameter electromechanical equivalent circuit model (EECM) for our proposed SPCT is established. The accuracy of the theoretical method is validated with the experimental method and the finite element method (FEM). On the basis of the electromechanical equivalent circuit, we investigate the voltage and power gains and electromechanical properties of our proposed design as functions of the load resistance and geometry size under different dielectric and

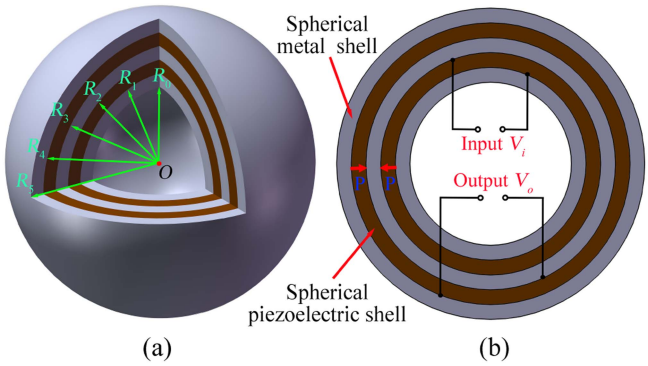

Fig. 1. (a) Three-dimensional schematic diagram of our proposed SPCT composed of five spherical shells stacking in the radial direction. (b) Working circuit in the cross-sectional view of the SPCT and the input and output spherical piezoceramic shells polarized in opposite directions.

mechanical losses. The experimentally measured voltage and power gains, resonance frequency, and antiresonance frequency for our proposed design are basically consistent with the analyzed and simulated results.

II. STRUCTURE AND PRINCIPLE

A. Structure of the SPCT

Fig. 1(a) demonstrates the diagrammatic sketch of the proposed SPCT, which consists of a five-layer concentric spherical shell with different radii, with two layers made of piezoelectric ceramic and three layers made of metal. The inner radius and outer radius of the inner, middle, and outer metal shells are denoted by R_0 and R_1, R_2 and R_3, and R_4 and R_5. The input and output piezoceramic shells are indicated by dark brown, whose inner radius and outer radius are R_1 and R_2 and R_3 and R_4, respectively. The material we use for piezoelectric ceramic is PZT-4, which is fragile. Therefore, we protect it by covering the piezoelectric ceramic spherical shell with a metal spherical shell, which is adjustable in thickness. Fig. 1(b) illustrates the working circuit in the cross-sectional view of the resulting device, where the inner and outer piezoceramic shells are set as the input end and output end of the ultrasonic wireless power transmission system. The input end is connected to an electric signal generator, while the output end is connected to a load resistor. Our mechanism is that when the excitation voltage is applied on the input spherical piezoelectric ceramic shell, the electric signal will convert to radial vibration, which propagates through the intermediate transmission spherical metal shell, and the radial vibration at the output spherical piezoceramic shell will convert to the electric signal because of the piezoelectric effect. It is worth stressing that the output voltage and power of our proposed wireless power transmission system can be modulated by applying different loads.

B. Analysis of EECM

In order to study the electromechanical characteristics of our proposed SPCT, we utilize an EECM including load mechanical impedances and mechanical and dielectric losses, as illustrated

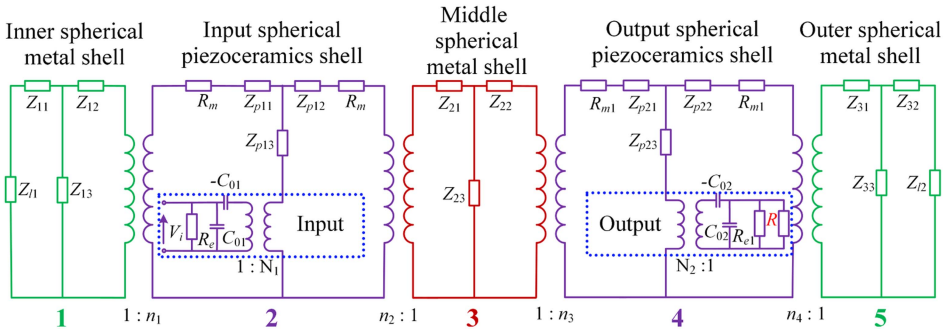

Fig. 2. EECM of the proposed SPCT.

in Fig. 2. The electromechanical equivalent circuit method is used to transform the mechanical vibration properties of piezoelectric elastomers into a theoretically more familiar circuit system by means of a force-electric analogy. The electromechanical equivalent circuits of the inner, middle, and outer metal shells are symbolized with Sections I, III, and V in Fig. 2, while Sections IV and II indicate the electromechanical equivalent circuits of the output and input piezoceramic shells. These five concentric spherical shells are connected in series from the inside to the outside at the mechanical end. As can be seen in Fig. 2, the equivalent circuits of the input and output piezoelectric ceramic spherical shells have electrical terminals, which are due to the piezoelectric effect. The input voltage and electric load resistance of the spherical piezoceramic transformer are indicated by $V_{\rm i}$ and R. The spherical piezoelectric transformer is based on the structural design of [30], so they have a relatively similar theoretical background. By using the constitutive equation, motion equation, and corresponding boundary conditions of the spherical metal shell, in previous work, we derived the series and parallel equivalent mechanical impedances of $Z_{1(2,3)1}$, $Z_{1(2,3)2}$, and $Z_{1(2,3)3}$. Their impedance expressions are shown as follows:

$$Z_{1(2,3)1} = \frac{a_{11}R_i^2 4\pi \mathrm{j}q\left(J_\alpha\left(qR_{i+1}\right)Y_{\alpha-1}\left(qR_i\right)-J_{\alpha-1}\left(qR_i\right)Y_\alpha\left(qR_{i+1}\right)\right)}{\omega\left(J_\alpha\left(qR_{i+1}\right)Y_\alpha\left(qR_i\right)-J_\alpha\left(qR_i\right)Y_\alpha\left(qR_{i+1}\right)\right)} + \frac{4\pi R_i \mathrm{j}\left(2a_{12}-a_{11}/2-\mu a_{11}\right)}{\omega} - \frac{8a_{11}\sqrt{R_i}\sqrt{R_{i+1}}\mathrm{j}}{\omega\left(J_\alpha\left(qR_{i+1}\right)Y_\alpha\left(qR_i\right)-J_\alpha\left(qR_i\right)Y_\alpha\left(qR_{i+1}\right)\right)} \quad (1)$$

$$Z_{1(2,3)2} = \frac{a_{11}R_{i+1}^2 4\pi \mathrm{j}q\left(J_\alpha\left(qR_i\right)Y_{\alpha-1}\left(qR_{i+1}\right)-J_{\alpha-1}\left(qR_{i+1}\right)Y_\alpha\left(qR_i\right)\right)}{\omega\left(J_\alpha\left(qR_{i+1}\right)Y_\alpha\left(qR_i\right)-J_\alpha\left(qR_i\right)Y_\alpha\left(qR_{i+1}\right)\right)} + \frac{4\pi R_{i+1}\mathrm{j}\left(-2a_{12}+a_{11}/2+\mu a_{11}\right)}{\omega} - \frac{8\mathrm{j}a_{11}\sqrt{R_i}\sqrt{R_{i+1}}}{\omega\left(J_\alpha\left(qR_{i+1}\right)Y_\alpha\left(qR_i\right)-J_\alpha\left(qR_i\right)Y_\alpha\left(qR_{i+1}\right)\right)} \quad (2)$$

$$Z_{1(2,3)3} = \frac{8\mathrm{j}a_{11}\sqrt{R_i}\sqrt{R_{i+1}}}{\omega\left(J_\alpha\left(qR_{i+1}\right)Y_\alpha\left(qR_i\right)-J_\alpha\left(qR_i\right)Y_\alpha\left(qR_{i+1}\right)\right)} \quad (3)$$

where R_i and R_{i+1} are the inner radius and outer radius of these spherical metal shells, $\alpha = \sqrt{(2(a_{22}+a_{23}-a_{12})/a_{11})+1/4}$, $a_{11}=a_{22}=E(1-\sigma_0)/k$, $a_{12}=a_{23}=E\sigma_0/k$, $k=(1+\sigma_0)(1-2\sigma_0)$, $V=\sqrt{a_{11}/\rho}$, $q=\omega/V$, V refers to the velocity of radial vibration, ρ represents the mass density, E indicates Young's modulus, σ_0 is the Poisson's ratio, and$J_\alpha(qR)$ and $Y_\alpha(qR)$ are the Bessel's functions of the first and second kinds.

The electromechanical equivalent circuits of the input and output spherical piezoelectric ceramic shells are represented by Sections II and IV in Fig. 2. Using the constitutive equation, motion equation, and corresponding boundary conditions of the spherical piezoelectric ceramic shell, in previous work we derived the series and parallel equivalent mechanical impedances of $Z_{p1(2)1}$, $Z_{p1(2)2}$, and $Z_{p1(2)3}$. Their impedance expressions can be obtained as follows [32], Eqs. (4) and (5) are shown at the bottom of the next page:

$$Z_{p1(2)3} = \frac{8\mathrm{j}\left(c_{33}+e_{33}^2/\varepsilon_{33}^3\right)R_iR_{i+1}\chi_a\chi_b}{\omega b_1} \quad (6)$$

where

$$\mu = \sqrt{2(c_{11}+c_{12}-c_{13}-e_{31}e_{33}/\varepsilon_{33}^s+2e_{31}^2/\varepsilon_{33}^{31})/(c_{33}+e_{33}^2/\varepsilon_{33}^3)+1/4}$$

$\lambda=\omega/c_1$, $c_1=\sqrt{(c_{33}+e_{33}^2/\varepsilon_{33}^3)/\rho_r}$, $\eta=-2e_{31}/(\varepsilon_{33}^{\rm s}(c_{33}+e_{33}^2/\varepsilon_{33}^3))$, and c_1 and ρ_r are the sound speed and mass density for our piezoceramic shell.

The series and parallel equivalent mechanical impedances for our piezoceramic shell, the specific parameters can be expressed as

$$\chi_a = \frac{e_{31}\sqrt{\lambda}}{\varepsilon_{33}b_1}\begin{pmatrix}2R_i\lambda\left(J_{\mu+1}\left(\lambda R_i\right)Y_\mu\left(\lambda R_{i+1}\right)\right.\\ \left.-Y_{\mu+1}\left(\lambda R_i\right)J_\mu\left(\lambda R_{i+1}\right)\right)\\ s_{-\frac{3}{2}\mu}\left(\lambda R_i\right)-\frac{4}{\pi}s_{-\frac{3}{2}\mu}\left(\lambda R_{i+1}\right)\\ +2R_i\lambda b_1\left(\mu+\frac{5}{2}\right)s_{-\frac{5}{2}\mu+1}\left(\lambda R_i\right)\end{pmatrix} - \frac{e_{33}}{\varepsilon_{33}}R_i^{-\frac{1}{2}} \quad (7)$$

$$\chi_b = \frac{e_{31}\sqrt{\lambda}}{\varepsilon_{33}b_1}\begin{pmatrix}\left(J_{\mu+1}\left(\lambda R_{i+1}\right)Y_\mu\left(\lambda R_i\right)\right.\\ \left.-Y_{\mu+1}\left(\lambda R_{i+1}\right)J_\mu\left(\lambda R_i\right)\right)s_{-\frac{3}{2}\mu}\left(\lambda R_{i+1}\right)\\ 2R_{i+1}\lambda-\frac{4}{\pi}s_{-\frac{3}{2}\mu}\left(\lambda R_i\right)\\ +2R_{i+1}\lambda b_1\left(\mu+\frac{5}{2}\right)s-\frac{5}{2}\mu+1\left(\lambda R_{i+1}\right)\end{pmatrix} - \frac{e_{33}}{\varepsilon_{33}}R_{i+1}^{-\frac{1}{2}} \quad (8)$$

$$\Delta = -\frac{1}{\varepsilon_{33}^{s}}\left(\frac{1}{R_{i+1}}-\frac{1}{R_i}\right)-\left(-2e_{31}/\left(\varepsilon_{33}^{\mathrm{s}}\left(c_{33}+e_{33}^2/\varepsilon_{33}^3\right)\right)\right)b_4 + \frac{b_2b_5}{b_1}-\frac{b_3b_6}{b_1} \tag{9}$$

where b_1, b_2, b_3, b_4, b_5, and b_6 are six constants, which originated from (9). They are constants of the voltage expression between the inner and outer electrodes of a spherical piezoelectric ceramic shell. Their values can be calculated according to the following equations:

$$b_1 = J_\mu(\lambda R_{i+1})\,Y_\mu(\lambda R_i) - J_\mu(\lambda R_i)\,Y_\mu(\lambda R_{i+1}) \tag{10}$$

$$b_2 = \eta\sqrt{\lambda}\left[s_{-\frac{3}{2},\mu}(\lambda R_{i+1})\,Y_\mu(\lambda R_i) - s_{-\frac{3}{2},\mu}(\lambda R_i)\,Y_\mu(\lambda R_{i+1})\right] \tag{11}$$

$$b_3 = \eta\sqrt{\lambda}\left[s_{-\frac{3}{2},\mu}(\lambda R_{i+1})\,J_\mu(\lambda R_i) - s_{-\frac{3}{2},\mu}(\lambda R_i)\,J_\mu(\lambda R_{i+1})\right] \tag{12}$$

$$b_4 = 2\frac{\mathrm{e}_{31}}{\varepsilon_{33}^{s}}\sqrt{\lambda}S + \frac{\mathrm{e}_{33}}{\varepsilon_{33}^{s}}\sqrt{\lambda}\left[R_{i+1}^{-\frac{1}{2}}s_{-\frac{3}{2}\mu}(\lambda R_{i+1}) - R_i^{-\frac{1}{2}}s_{-\frac{3}{2}\mu}(\lambda R_i)\right] \tag{13}$$

$$b_5 = 2\frac{\mathrm{e}_{31}}{\varepsilon_{33}^{s}}\sqrt{\lambda}J + \frac{\mathrm{e}_{33}}{\varepsilon_{33}^{s}}\sqrt{\lambda}\left[R_{i+1}^{-\frac{1}{2}}J_\mu(\lambda R_{i+1}) - R_i^{-\frac{1}{2}}J_\mu(\lambda R_i)\right] \tag{14}$$

$$b_6 = 2\frac{\mathrm{e}_{31}}{\varepsilon_{33}^{s}}\sqrt{\lambda}Y + \frac{\mathrm{e}_{33}}{\varepsilon_{33}^{s}}\sqrt{\lambda}\left[R_{i+1}^{-\frac{1}{2}}Y_\mu(\lambda R_{i+1}) - R_i^{-\frac{1}{2}}Y_\mu(\lambda R_i)\right]. \tag{15}$$

The other introduced parameters in the expressions can be expressed as follows:

$$S = \frac{1}{(\mu/2+1/4)(\mu/2-1/4)} \times \begin{pmatrix} \frac{{}_2F_3\left(\left[-\frac{1}{2},1\right],\left[\frac{1}{2},-\frac{1}{2}\mu+\frac{3}{4},\frac{1}{2}\mu+\frac{3}{4}\right],-\frac{1}{4}R_{i+1}^2\lambda^2\right)}{4\sqrt{\lambda R_{i+1}}} \\ -\frac{{}_2F_3\left(\left[-\frac{1}{2},1\right],\left[\frac{1}{2},-\frac{1}{2}\mu+\frac{3}{4},\frac{1}{2}\mu+\frac{3}{4}\right],-\frac{1}{4}R_i^2\lambda^2\right)}{4\sqrt{\lambda R_i}} \end{pmatrix}$$

$$J = \frac{\sqrt{2\lambda}}{4}\left\{\frac{\sqrt{2}R^{-\frac{1}{2}}\lambda^{-\frac{1}{2}}\left[4R^2\lambda^2+(2\mu+1)(3+2\mu)\right]J_\mu(\lambda R)}{(\mu/2-1/4)(2\mu+1)(3+2\mu)} - \frac{2\sqrt{2}R^{\frac{1}{2}}\lambda^{\frac{1}{2}}J_{\mu+1}(\lambda R)}{(\mu/2-1/4)(2\mu+1)} - \frac{4\sqrt{2}R\lambda J_\mu(\lambda R)s_{\frac{3}{2}\mu}(\lambda R)}{(\mu/2-1/4)(2\mu+1)(3+2\mu)} + \frac{2\sqrt{2}R\lambda J_{\mu+1}(\lambda R)s_{\frac{1}{2}\mu}(\lambda R)}{(\mu/2-1/4)(2\mu+1)}\right\}\Bigg|_i^{i+1}$$

$$Y = \frac{\sqrt{2\lambda}}{4}\left\{\frac{\sqrt{2}R^{-\frac{1}{2}}\lambda^{-\frac{1}{2}}\left[4R^2\lambda^2+(2\mu+1)(3+2\mu)\right]Y_\mu(\lambda R)}{(\mu/2-1/4)(2\mu+1)(3+2\mu)} - \frac{2\sqrt{2}R^{\frac{1}{2}}\lambda^{\frac{1}{2}}Y_{\mu+1}(\lambda R)}{(\mu/2-1/4)(2\mu+1)} - \frac{4\sqrt{2}R\lambda Y_\mu(\lambda R)s_{\frac{3}{2},\mu}(\lambda R)}{(\mu/2-1/4)(2\mu+1)(3+2\mu)} + \frac{2\sqrt{2}R\lambda Y_{\mu+1}(\lambda R)s_{\frac{1}{2}\mu}(\lambda R)}{(\mu/2-1/4)(2\mu+1)}\right\}\Bigg|_i^{i+1}$$

where $s_{\frac{3}{2},\mu}(\lambda R)$ indicates the first kind of Lommel function. $J_\mu(\lambda R)$, $Y_\mu(\lambda R)$, and ${}_mF_n$ ($[a_1 \ldots a_m]$, $[\beta_1 \ldots \beta_m]$, x) are Bessel's functions of the first and second kinds and the generalized hypergeometric function. $\chi = 1/\Delta$, $\mathrm{N}_{1(2)} = 4\pi\chi\sqrt{R_{i+1}}\sqrt{R_i}\chi_a\chi_b$, $C_{01(2)} = 4\pi\chi$, $n_{1(3)} = R_{i+1}\chi_b$, and $n_{2(4)} = R_i\chi_a.\mathrm{N}_{1(2)}$ refers to the electromechanical conversion coefficient, and $C_{01(2)}$ represents the clamped capacitance.

The input mechanical impedances of the front and back metal shells are

$$Z_{\mathrm{m}i} = Z_{12} + \frac{(Z_{11}+Z_{l1})Z_{13}}{(Z_{11}+Z_{l1})+Z_{13}} \tag{16}$$

$$Z_{\mathrm{mo}} = Z_{31} + \frac{(Z_{32}+Z_{l2})Z_{33}}{(Z_{32}+Z_{l2})+Z_{33}} \tag{17}$$

$$\begin{aligned} Z_{p1(2)1} = {} & \frac{\mathrm{j}4\pi R_iR_{i+1}\chi_b^2\left(\left(2c_{31}+2e_{33}e_{31}/\varepsilon_{33}^3\right)-\left(c_{33}+e_{33}^2/\varepsilon_{33}^3\right)/2-\left(c_{33}+e_{33}^2/\varepsilon_{33}^3\right)\mu\right)}{\omega} \\ & + \frac{\mathrm{j}4\pi R_i^2R_{i+1}\chi_b^2\left(c_{33}+e_{33}^2/\varepsilon_{33}^3\right)\lambda\left(J_\mu(\lambda R_{i+1})Y_{\mu-1}(\lambda R_i)-Y_\mu(\lambda R_{i+1})J_{\mu-1}(\lambda R_i)\right)}{\omega b_1} \\ & - \frac{8\mathrm{j}\left(c_{33}+e_{33}^2/\varepsilon_{33}^3\right)R_iR_{i+1}\chi_a\chi_b}{\omega b_1} \end{aligned} \tag{4}$$

$$\begin{aligned} Z_{p1(2)2} = {} & \frac{\mathrm{j}4\pi R_iR_{i+1}\chi_a^2\left(-\left(2c_{31}+2e_{33}e_{31}/\varepsilon_{33}^3\right)+\left(c_{33}+e_{33}^2/\varepsilon_{33}^3\right)/2+\left(c_{33}+e_{33}^2/\varepsilon_{33}^3\right)\mu\right)}{\omega} \\ & + \frac{\mathrm{j}4\pi R_{i+1}^2R_i\chi_a^2\left(c_{33}+e_{33}^2/\varepsilon_{33}^3\right)\lambda\left(J_\mu(\lambda R_i)Y_{\mu-1}(\lambda R_{i+1})-Y_\mu(\lambda R_i)J_{\mu-1}(\lambda R_{i+1})\right)}{\omega b_1} \\ & - \frac{8\mathrm{j}\left(c_{33}+e_{33}^2/\varepsilon_{33}^3\right)R_iR_{i+1}\chi_a\chi_b}{\omega b_1} \end{aligned} \tag{5}$$

where the load mechanical impedances of the inner and outer terminals are Z_{l1} and Z_{l2}. When our proposed SPCT is not subjected to external force, the load mechanical impedances of the inner and outer terminals are equal to zero.

The input electric impedance for our output piezoceramic shell is

$$Z_6 = \frac{R + R_{e1}}{\omega^2 C_{02}^2 R R_{e1} - (R + R_{e1})\, j\omega C_{02}} \tag{18}$$

where R and R_{e1} are the electric load resistance and dielectric loss equivalent resistance, respectively.

The reflected mechanical impedance for the output piezoceramic shell can be obtained as follows:

$$Z_5 = \mathrm{N}_2^2 Z_6. \tag{19}$$

The input mechanical impedance at the contacting surface between the spherical middle metal shell and the output piezoelectric ceramic shell can be derived out

$$Z_4 = R_{m1} + Z_{\mathrm{p21}} + \frac{\left(Z_{\mathrm{mo}} n_4^2 + R_{m1} + Z_{\mathrm{p22}}\right)\left(Z_5 + Z_{\mathrm{p23}}\right)}{Z_{\mathrm{mo}} n_4^2 + R_{m1} + Z_{\mathrm{p22}} + Z_5 + Z_{\mathrm{p23}}} \tag{20}$$

where R_{m1} is the mechanical loss equivalent resistance for the output piezoceramic shell.

The input mechanical impedance at the contacting surface between the input spherical piezoelectric ceramic shell and the middle metal shell can be given as

$$Z_3 = Z_{21} + \frac{\left(Z_4/n_3^2 + Z_{22}\right) Z_{23}}{Z_4/n_3^2 + Z_{22} + Z_{23}}. \tag{21}$$

The equivalent mechanical impedance for the spherical piezoceramic transformer at the mechanical terminal can be given as

$$Z_2 = Z_{\mathrm{p13}} + \frac{\left(Z_{\mathrm{mi}} n_1^2 + R_m + Z_{\mathrm{p11}}\right)\left(Z_3 n_2^2 + R_m + Z_{\mathrm{p12}}\right)}{Z_{\mathrm{mi}} n_1^2 + 2R_m + Z_{\mathrm{p11}} + Z_3 n_2^2 + Z_{\mathrm{p12}}}. \tag{22}$$

The input electric impedance of the SPCT can be given as

$$Z_{\mathrm{ie}} = R_{\mathrm{ie}} + jX_{\mathrm{ie}} = \frac{R_{\mathrm{e}}\left(\mathrm{N}_1^2 - j\omega C_{01} Z_2\right)}{\left(\mathrm{N}_1^2 - j\omega C_{01} Z_2\right) + \omega^2 C_{01}^2 R_e Z_2}. \tag{23}$$

By setting the imaginary part of the input electric impedance and the imaginary part of the input electric admittance to zero, the equations for the resonance frequency and antiresonance frequency are obtained

$$X_{\mathrm{ie}} = 0 \tag{24}$$

$$\frac{X_{\mathrm{ie}}}{R_{\mathrm{ie}}^2 + X_{\mathrm{ie}}^2} = 0. \tag{25}$$

When the resonance and antiresonance frequencies are given, the effective electromechanical coupling coefficient for our proposed spherical piezoceramic transformer can be given as

$$k_{\mathrm{eff}} = \sqrt{1 - f_{\mathrm{r}}^2 / f_{\mathrm{a}}^2}. \tag{26}$$

The voltage gain for our proposed spherical piezoceramic transformer defined as the output voltage across load electric impedance divided by the voltage of input piezoceramic shell can be given as

$$\mathrm{G_V} = \frac{V_o}{V_i} = \frac{R}{Z_{\mathrm{ie}}} \times \mathrm{Z_P}. \tag{27}$$

The detailed expression of $\mathrm{Z_P}$ can be expressed as follows:

$$\begin{aligned}\mathrm{Z_P} = {} & \frac{Z_{\mathrm{C02}}}{R + Z_{\mathrm{C02}}} \times \frac{Z_{\mathrm{p22}} + R_{m1} + Z_{\mathrm{mo}} n_4^2}{Z_5 + Z_{\mathrm{p23}} + Z_{\mathrm{p22}} + R_{m1} + Z_{\mathrm{mo}} n_4^2} \times \frac{\mathrm{N}_2}{\mathrm{N}_1} \\ & \times \frac{Z_{23}}{Z_4/\mathrm{n}_3^2 + Z_{23} + Z_{22}} \times \frac{\mathrm{n}_2}{\mathrm{n}_3} \times \frac{Z_{\mathrm{C01}}}{Z_2/\mathrm{N}_1^2 - 1/\left(j\omega C_{01}\right) + Z_{\mathrm{C01}}} \\ & \times \frac{Z_{\mathrm{p11}} + R_m + Z_{\mathrm{mi}} n_1^2}{Z_3 n_2^2 + Z_{\mathrm{p12}} + Z_{\mathrm{p11}} + 2R_m + Z_{\mathrm{mi}} n_1^2}\end{aligned} \tag{28}$$

where $Z_{\mathrm{C01}} = \frac{R_e}{1 + j\omega C_{01} R_e}$, $Z_{\mathrm{C02}} = \frac{R_{e1}}{1 + j\omega C_{02} R_{e1}}$, and Z_{C01} and Z_{C02} are the clamped capacitance for the input and output spherical piezoelectric ceramic shells.

The power gain for our presented spherical piezoceramic transformer can be expressed as

$$\mathrm{G_p} = \frac{P_o}{P_i} = \frac{V_o^2}{V_i^2} \times \frac{Z_{\mathrm{ie}}}{R} = \mathrm{G_V^2} \times \frac{Z_{\mathrm{ie}}}{R}. \tag{29}$$

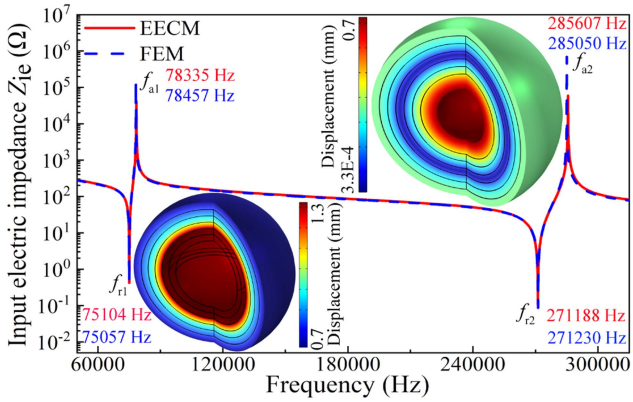

Fig. 3. Input electric impedance for our presented SPCT. Inserts: Corresponding first and second radial vibration modes.

III. Analysis of Performance Parameter of SPCT

A. Input Electric Impedance and Vibration Modes

In this article, we perform the numerical simulations utilizing the Electrostatics Module, Solid Mechanics Module, and Circuit Module in COMSOL Multiphysics. Fig. 3 depicts the variation of input electric impedance with frequency, where the input spherical piezoceramic shell exerts a 1 V excitation voltage and the output spherical piezoceramic shell is open-circuited. The red line and the blue dashed line indicate the EECM and FEM results. The material parameters of the proposed SPCT are set as follows: $R_0 = 11$ mm, $R_1 = 13$ mm, $R_2 = 15$ mm, $R_3 = 17$ mm, $R_4 = 19$ mm, and $R_5 = 21$ mm, wherein the metal shells are made of 7050 aluminum possessing the standard parameters of $\mathrm{E} = 7 \times 10^{10}$ Pa, $\rho = 2700$ kg/m^3, and $\sigma_0 = 0.33$. For the piezoelectric ceramic shell, the material we use for the piezoelectric ceramic is PZT-4. The standard material parameters are $\rho_r = 7.5 \times 10^3$ kg/m^3, $c_{11}^E = 7.43 \times 10^{10}$ N/m^2,

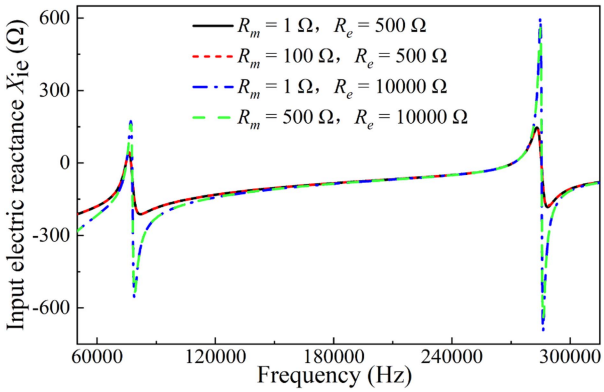

Fig. 4. Input electric reactance as a function of frequency.

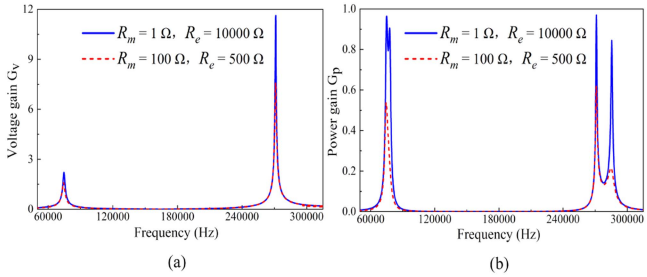

Fig. 5. Frequency dependence of (a) voltage gain and (b) power gain with different mechanical and dielectric losses.

$c_{12}^E = 7.78 \times 10^{10}$ N/m^2, $c_{13}^E = 12.3 \times 10^{10}$ N/m^2, $c_{33}^E = 7.78 \times 10^{10}$ N/m^2, e_{31} = -5.2 N/(mV), e_{33} = 15.1 N/(mV), and $\varepsilon_{33}^S = 5.62 \times 10^{-9}$ F/m. The first resonance frequency and antiresonance frequency for EECM and FEM results are 75 104 Hz, 78 335 Hz and 75 057 Hz, 78 457 Hz. The relative errors of these two aforementioned results are 0.001% and 0.002%. The second resonance frequency and antiresonance frequency for EECM and FEM results are 271 188 Hz, 285 607 Hz and 271 230 Hz, 285 050 Hz, respectively. Their relative errors are 0.0001% and 0.002%. The first and second radial vibration modes are displayed in the bottom left and top right panels, where the first mode shape of our presented SPCT is a breathing vibration mode, while the displacement node of the second radial vibration mode is placed at the center of the radial dimension. In what follows, we will analyze the influence of mechanical and dielectric losses on the electromechanical properties and voltage and power gain of our proposed SPCT.

B. Input Electric Reactance With Different Mechanical and Dielectric Losses

Fig. 4 demonstrates the variation of input electric reactance with the frequency under different mechanical losses and dielectric losses under the electric load resistance of 300 Ω. When the input electric reactance is zero, it is the resonance frequency of the SPCT. In the current study, we evaluated the losses of the spherical piezoelectric transformer by introducing mechanical and dielectric losses. Mechanical and dielectric losses represent the thermal energy losses of the transformer. Mechanical loss arises from internal friction during mechanical vibration or deformation of the transformer material, and dielectric loss is the energy loss caused by the polarization hysteresis of piezoelectric ceramics in an alternating electric field. Generally speaking, a small R_m implies a small mechanical loss, and a large R_e implies a small dielectric loss. When the mechanical loss is fixed at 1 Ω, the resonance frequencies of our proposed SPCT are 75 046 and 75 104 Hz, corresponding to the dielectric losses of 500 and 10 000 Ω. When the dielectric loss is chosen as 10 000 Ω, the input electric reactance curve corresponding to a mechanical loss of 500 Ω is smaller at the peak than the reactance curve corresponding to a mechanical loss of 1 Ω. At the same time, they both have a resonance frequency of 75 046 Hz. It can be concluded that under the same dielectric loss value, the greater the mechanical loss, the smaller the peak value of the input reactance curve, and under the same mechanical loss value, the peak value of the input reactance will increase with the increase of the dielectric loss.

C. Voltage and Power Gains for Our Presented SPCT

Fig. 5(a) illustrates the voltage gain curves of our spherical piezoceramic transformer with different losses, where an electrical load resistance of 300 Ω is applied. The first and second maximum values correspond to the first- and second-order resonance frequencies of 74 250 Hz and 271 046 Hz, under the mechanical loss of 100 Ω and the dielectric loss of 500 Ω. When the mechanical and dielectric losses are set as 1 Ω and 10 000 Ω, the first two maximum voltage gains are located at resonance frequencies of 74 663 and 271 128 Hz. As can be seen from the figure, when the dielectric loss decreases and the mechanical loss increases, the resonance frequency of our proposed SPCT remains almost unchanged while the value of the voltage gain decreases. Fig. 5(b) displays the power gain of our proposed SPCT under various mechanical loss and dielectric loss conditions, in which the electric load resistance is chosen as 300 Ω. The power gain of the resulting device reaches its maximum values near the resonance frequency and antiresonance frequency. Since we take mechanical loss and dielectric loss into consideration, the power gain at the resonance frequency will not reach unity. It can be observed that the values of power gain at the first and second resonance frequencies are larger than those at the first and second antiresonance frequencies. Besides, the distance between two power gain peaks at the first resonance and antiresonance frequencies is smaller than that of the second resonance and antiresonance frequencies. At the first vibration mode, the two power gain peaks gradually merge into one peak as the mechanical loss increases and the dielectric loss decreases.

D. Effect of the Intermediate Transmission Metal Shell Thickness on the Electromechanical Characteristics

As analyzed above, the performance parameters of our proposed SPCT can be manipulated by adjusting its geometrical dimensions. Fig. 6(a) depicts the variation of resonance frequency and antiresonance frequency with the thickness of

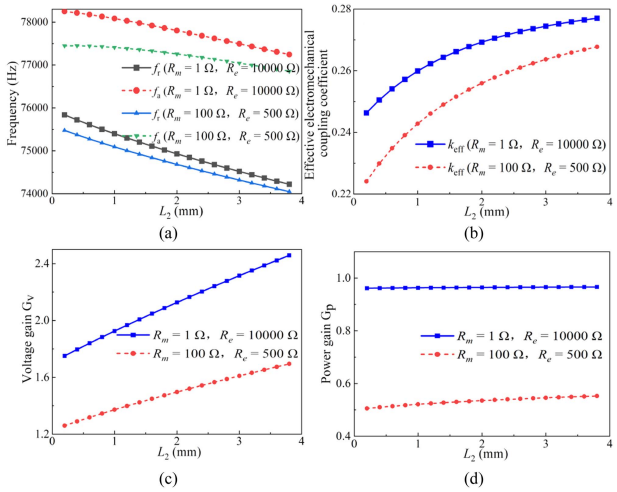

Fig. 6. (a) First-order resonance frequency and antiresonance frequency, (b) effective electromechanical coupling coefficients, (c) voltage gain, and (d) power gain as functions of the intermediate transmission spherical metal shell thickness with different losses.

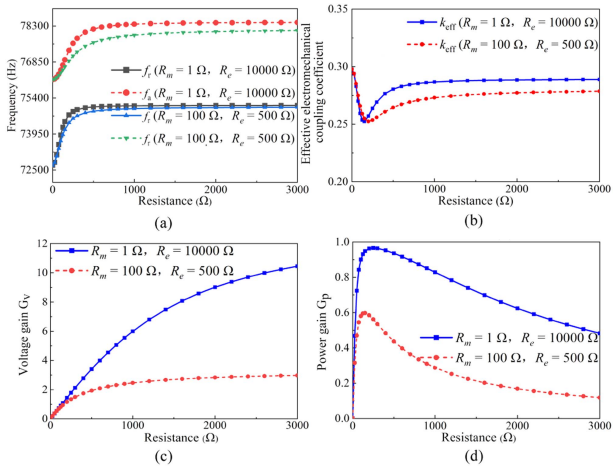

Fig. 7. (a) First-order resonance and anti-resonance frequencies, (b) effective electromechanical coupling coefficients, (c) voltage gain, and (d) power gain as a function of load resistance with different losses.

the intermediate transmission spherical metal shell, where L_2 represents the thickness of the intermediate metal shell, and the electric load resistance is set at 300 Ω. The parameters R_0, R_1, and R_2 of our proposed SPCT are kept constant. The total thickness and the thickness of the output piezoceramic shell are also fixed. This means that the thickness of the intermediate metal shell increases while the thickness of the outer metal shell decreases when L_2 increases. Since the elastic stiffness of the metal shell is less than that of the piezoceramic shell, when the output piezoceramic shell moves to the edge of the spherical piezoceramic transformer, the equivalent elastic stiffness of the spherical piezoceramic transformer becomes larger, and thus the first and second orders resonance frequency and antiresonance frequency decrease. The variation of the intermediate metal shell thickness with the effective electromechanical coupling coefficients under different losses is illustrated in Fig. 6(b), where the increment tends to be saturated as the L_2 increases. Fig. 6(c) demonstrates the relationship between L_2 and the voltage gain of our proposed design. When the thickness of the intermediate metal shell is increased, the voltage gain curve at 1 Ω mechanical loss and 10 000 Ω dielectric loss is larger than that at 100 Ω mechanical loss and 500 Ω dielectric loss, respectively. Fig. 6(d) describes the thickness of the intermediate spherical metal shell as a function of the power gain under different losses. When the parameter L_2 is increased, the value of voltage gain at 1 Ω mechanical loss and 10 000 Ω dielectric loss almost reaches unity and remains constant. When the mechanical loss is 100 Ω and the dielectric loss is 500 Ω, the voltage gain increases slightly. Therefore, the performance parameters of our proposed spherical piezoceramic transformer could be optimized via modulating the thickness of the intermediate metal shell.

E. Influence of Load Resistance on Electromechanical Characteristics

We investigate the variation of the electric load resistance with the first-order resonance frequency, antiresonance frequency, and k_{eff}, as demonstrated in Fig. 7(a) and (b), which is highly desired in practical applications. The output end of the resulting device is connected to a load resistance of 300 Ω, and the load resistance applied to the output end is changeable. The resonance frequency and antiresonance frequency increase rapidly, while the electromechanical coupling coefficient decreases rapidly, as the electric load resistance is relatively small (∼200 Ω). When the electric load resistance reaches a certain extent, the increments of the first-order resonance frequency and antiresonance frequency and k_{eff} will gradually decrease and tend to reach saturation. Fig. 7(c) illustrates the variation of the voltage gain of our proposed SPCT with the electric load resistance with different mechanical loss and dielectric loss, where the blue line and the red dashed line represent the mechanical loss and dielectric loss of 1 Ω, 10 000 Ω and 100 Ω, 500 Ω, respectively. The results show that the growth rate of voltage gain with different losses is almost the same when the electric load resistance is comparatively small. With the increase of load resistance, the difference in voltage gain between the two cases with different mechanical and dielectric losses becomes gradually larger. The efficiency of the SPCTs can be evaluated via the power gain. The variation in the electric load resistance has a particular impact on the power gain of our proposed SPCT under different losses, as illustrated in Fig. 7(d). It is observed that the power gain reaches its maximum value with the load resistance of ∼200 Ω, and then decreases gradually.

IV. Experimental Details

A. Measurement of the Resonance/Antiresonance Frequencies

To verify the correctness of the theoretical method, we fabricate a prototype and carry out an experiment to demonstrate the effectiveness of our proposed design. The experimental sample is made of a two-layer piezoelectric ceramic shell and a three-layer metal shell, where the sizes of the SPCT are $R_0 =$ 11 mm, $R_1 = 13$ mm, $R_2 = 15$ mm, $R_3 = 16$ mm, $R_4 = 18$ mm, and $R_5 = 20$ mm. Fig. 8(a) and (b) shows the experimental

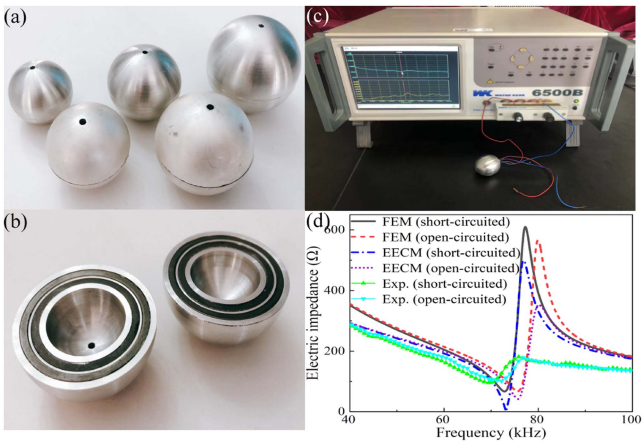

Fig. 8. (a) and (b) Photo of the experimental samples of the spherical piezoelectric transform. (c) Experimental setup to measure the electrical impedance of our proposed SPCT. (d) Relationship between the theoretically analyzed, numerically simulated, and experimentally measured electrical impedance and frequency.

samples of the spherical piezoceramic transform, where the piezoceramic and metal shells have a hole to connect the electrodes. In the manufacturing process of the SPCT, we glue two inner hemispherical metal shells together by using conductive adhesive to form an inner spherical metal shell. A clamp is used to tightly secure the inner spherical metal shell until the conductive adhesive solidifies. Then we use the epoxy resin adhesive for bonding two input hemispherical piezoceramic shells, and the negative and positive electrodes are glued on the inner surface and outer surface of the input piezoceramic shell. We use epoxy resin adhesive to glue two piezoelectric ceramic hemispheres in order to prevent the inner and outer electrodes from conducting. Subsequently, two middle metal hemispheres are glued to the input piezoelectric ceramic sphere with epoxy resin adhesive. Using the same approach, other piezoceramic and metal shells are coated on the input piezoceramic shell for building the ultimate SPCT. When bonding the metal and piezoelectric ceramic spherical shells, we used a conductive adhesive and fixed each layer of the structure with a clamp to avoid interlayer air bubbles. Between the two electrodes is aluminum instead of an insulating medium, so we neglected the effect of parasitic capacitance. The standard material parameters utilized in experiments are the same as those utilized in the aforementioned analysis. Fig. 8(c) demonstrates the experimental setup for measuring the input electric impedance for our proposed spherical piezoceramic transformer prototype. A WK6500B precision impedance analyzer is used to measure the frequency dependence of the input electric impedance. Fig. 8(d) illustrates the theoretically analyzed, numerically simulated, and experimentally measured electrical impedance of our designed SPCT. For simplicity and without loss of generality, we consider two limiting electric load resistance cases, one of which is short-circuited and the other is open-circuited. The mechanical loss of 100 Ω and the dielectric loss of 500 Ω are utilized in the theoretical analysis. Due to the different way of adding losses in COMSOL Multiphysics than in EECM, we introduce the isotropic mechanical damping of 0.075 and the isotropic dielectric loss factor of 0.005 into the numerical simulations, which have roughly the same electromechanical characteristics as the losses used in EECM [28]. In practical engineering applications, the losses of piezoelectric transformers are difficult to quantify and measure, so they can only be predicted approximately by theory and the FEM. The theoretically analyzed, numerically simulated, and experimental resonance frequency and antiresonance frequency for our proposed SPCT are listed in Table II, where f_r,f_a,f_{rs},f_{as},f_{rm}, and f_{am} are the theoretical, simulated, and experimental resonance frequency and antiresonance frequency. $\Delta_1 = |f_r - f_{rs}|/f_r$, $\Delta_2 = |f_r - f_{rm}|/f_r$, $\Delta_3 = |f_a - f_{as}|/f_a$, and $\Delta_4 = |f_a - f_{am}|/f_a$ are the relative errors. The resonance frequency and antiresonance frequency calculated by different methods are basically consistent with the results obtained by experiments. The experimental results differ from FEM and EECM results mainly due to the unavoidable manufacturing and installation errors in the fabrication of the spherical piezoelectric transformer. In the manufacturing process, each layer of metal and piezoceramic shell has a small hole to lead the wires, which was not taken into consideration in theoretical calculations and finite element simulations. Besides, the radius tolerance for machining the spherical metal shell is 0.02 mm, and there are more or less differences between actual material parameters and standard material parameters.

TABLE II
THEORETICAL, SIMULATED, AND EXPERIMENTAL RESONANCE FREQUENCY AND ANTIRESONANCE FREQUENCY FOR OUR PROPOSED SPCT

Case	R (Ω)	f_r (Hz)	f_{rs} (Hz)	f_{rm} (Hz)	Δ_1 (%)	Δ_2 (%)
Resonance frequency	0	73 152	72 840	69 478	0.43	5.02
	∞	75 669	75 620	72 205	0.06	4.58
	R (Ω)	f_a (Hz)	f_{as} (Hz)	f_{am} (Hz)	Δ_3 (%)	Δ_4 (%)
Anti resonance frequency	0	76 904	77 260	75 841	0.46	1.38
	∞	80 164	79 950	76 750	0.27	4.26

B. Measuring Voltage and Power Gains of the Proposed SPCT

Fig. 9(a) demonstrates the experimental setup for measuring the voltage gain of our presented spherical piezoceramic transformer. In the figure, a RIGOL DG1022U function generator with a 20 V peak-to-peak value output voltage is employed to stimulate our wireless power transmission system, and no power amplifier is used. Two Agilent 34401-A digital multimeters with an input impedance of 1 MΩ are employed for measuring the input voltage and output voltage. Fig. 9(b) illustrates the theoretically analyzed, numerically simulated, and experimentally measured voltage gain of the SPCT. In the experiment, the electric single frequency of the arbitrary waveform generator is kept at 71 596 Hz with an electric load resistance of 300 Ω. In the calculations, the same mechanical loss of 100 Ω and dielectric loss of 500 Ω are used in the electromechanical equivalent circuit method, and the isotropic mechanical damping of 0.075 and the isotropic dielectric loss factor of 0.005 are used in the

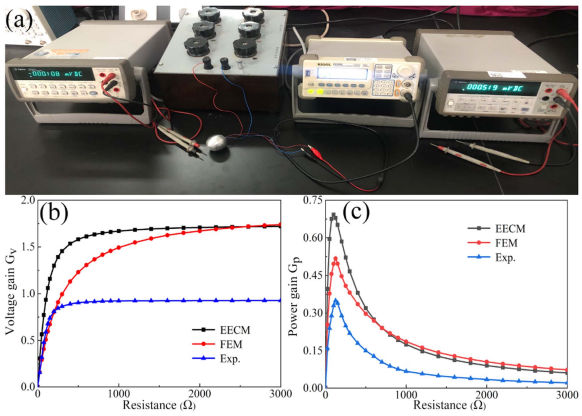

Fig. 9. (a) Photo of the experimental setup for the measurement of the voltage gain. The theoretically analyzed, numerically simulated, and experimentally measured (b) voltage gain and (c) power gain of the resulting device.

numerical simulation. The corresponding theoretically analyzed and numerically simulated resonance frequencies are 74 516 Hz and 75 453 Hz, respectively, when the output end of the resulting device is applied with a 300 Ω electric load resistance. As load resistance is relatively small, our spherical piezoceramic transformer voltage gain increases faster. The increment of the voltage gain tends to saturate with the gradual increase in the load resistance. The theoretical, simulated, and measured power gain of the proposed SPCT is demonstrated in Fig. 9(c), where the black, red, and blue lines represent the EECM, FEM, and experimental results, respectively. The power gain can be regarded as the transformer efficiency of our proposed design. The measured trend of the power gain is basically consistent with the theoretical and simulated results, and the power gain reaches its peak value as the electric load resistance is approximately 125 Ω. In the current study, the discrepancies between the EECM and FEM results arise primarily from differing loss representations. In the theoretical model, the mechanical and dielectric losses are expressed in equivalent resistance, whereas in the COMSOL finite element software, they need to be represented by loss factors. Therefore, there is a slight deviation between the EECM and FEM results. Since each layer of the spherical transformer has a small hole for the wires to pass through, we did not consider these small holes in our theoretical and numerical simulations, which cause slight deviations in the experimental results. In addition, assembly errors are inevitable when we manufacture the SPCT. Although we use a fixture to clamp each layer of the spherical shell when manufacturing the SPCT, minor interlayer bubbles may form during assembly, influencing experimental outcomes. Although we did not measure Bode plots for our spherical piezoelectric transformer, we measured the power and voltage gains of the spherical piezoelectric transformer as a function of electric load resistance. Measuring the Bode plot of the piezoelectric transformer will be the goal of our future work.

V. Conclusion

In conclusion, we systematically design and experimentally realize a spherical piezoceramic transformer consisting of five-layer concentric spherical shells, two of which are made of piezoelectric ceramic and three of which are made of metal. The exact electromechanical equivalent circuit of the proposed SPCT is deduced. When different dielectric and mechanical losses are considered, the electromechanical characteristics, voltage gain, and power gain of the proposed spherical piezoelectric transformer as functions of the electric load resistance and geometry size are investigated, which can be helpful for parameter optimization for some applications, such as wireless charging, power adapters, and backlight power supplies. The results show that for the same value of dielectric loss, the peak value of the input reactance curve is smaller when the mechanical loss is larger, while the peak value of the input reactance increases with the increase of dielectric loss for the same value of mechanical loss. When the intermediate metal shell thickness increases, the first-order resonance frequency and antiresonance frequency decrease, while the electromechanical coupling coefficients and the voltage gain increase. As the electric load resistance of our proposed SPCT increases, the voltage gain, resonance frequency, and antiresonance frequency increase. When the input voltage of a function generator is 20 V peak-to-peak and the load resistance is 125 Ω, the power gain, i.e., efficiency, of our proposed SPCT can reach about 36%. We display a reasonable agreement between the theoretical predictions and measured results, which provides evidence that our proposed design can realize step-up and step-down voltage conversion. In the current study, the main contribution of this article is to present a new concept of spherical piezoelectric transformers. In future work, we will employ optimization algorithms to enhance the performance of the SPCT and further refine the manufacturing methods for the SPCT. We anticipate that our methodology will provide the potential for designing the SPCT and may have profound and substantial implications in a variety of application scenarios, such as solar power equipment, portable electronic chargers, and battery chargers for mobile phones.

References

[1] S. Agarwal and E. Yablonovitch, "A nanoscale piezoelectric transformer for low-voltage transistors," *Nano Lett.*, vol. 14, no. 11, pp. 6263–6268, 2014.

[2] M. Khanna, R. Burgos, Q. Wang, K. D. Ngo, and A. V. Carazo, "New tunable piezoelectric transformers and their application in DC–DC converters," *IEEE Trans. Power Electron.*, vol. 32, no. 12, pp. 8974–8978, Dec. 2017.

[3] J. Yang, "Piezoelectric transformer structural modeling-A review," *IEEE Trans. Ultrasonics, Ferroelect., Freq. Control*, vol. 54, no. 6, pp. 1154–1170, Jun. 2007.

[4] A. Vazquez Carazo, "Piezoelectric transformers: An historical review," *Actuators*, vol. 5, no. 2, 2016, Art. no. 12.

[5] L. Wang, K. Sun, and R. Burgos, "Planar piezoelectric transformer-based high step-down voltage-ratio DC–DC converter," *IEEE Trans. Power Electron.*, vol. 37, no. 9, pp. 10833–10848, Sep. 2022.

[6] D. J. Falimiaramanana, F. E. Ratolojanahary, J.-E. Lefebvre, L. El Maimouni, and M. Rguiti, "2-D modeling of Rosen-type piezoelectric transformer by means of a polynomial approach," *IEEE Trans. Ultrasonics, Ferroelect., Freq. Control*, vol. 67, no. 8, pp. 1701–1714, Aug. 2020.

[7] Z. Yang, J. Forrester, J. N. Davidson, M. P. Foster, and D. A. Stone, "Resonant current estimation and phase-locked loop feedback design for piezoelectric transformer-based power supplies," *IEEE Trans. Power Electron.*, vol. 35, no. 10, pp. 10466–10476, Oct. 2020.

[8] S.-H. Kweon, K. Tani, K. Kanda, S. Nahm, and I. Kanno, "Piezoelectric PZT thin-film transformers with a ring–dot structure," *Jpn. J. Appl. Phys.*, vol. 59, no. SP, 2020, Art. no. SPPD09.
[9] J. D. Boles, E. Ng, J. H. Lang, and D. J. Perreault, "DC–DC converter implementations based on piezoelectric transformers," *IEEE J. Emerg. Sel. Topics Power Electron.*, vol. 10, no. 6, pp. 6754–6769, Dec. 2021.
[10] J. D. Boles, J. E. Bonavia, P. L. Acosta, Y. K. Ramadass, J. H. Lang, and D. J. Perreault, "Evaluating piezoelectric materials and vibration modes for power conversion," *IEEE Trans. Power Electron.*, vol. 37, no. 3, pp. 3374–3390, Mar. 2021.
[11] J. Forrester, J. N. Davidson, M. P. Foster, and D. A. Stone, "Influence of spurious modes on the efficiency of piezoelectric transformers: A sensitivity analysis," *IEEE Trans. Power Electron.*, vol. 36, no. 1, pp. 617–629, Jan. 2021.
[12] Y. Yuanmao, K. E. Cheng, and K. Ding, "A novel method for connecting multiple piezoelectric transformer converters and its circuit application," *IEEE Trans. Power Electron.*, vol. 27, no. 4, pp. 1926–1935, Apr. 2012.
[13] Y. Du et al., "Two-dimensional equivalent circuit model of ultrasonic wireless power transmission," *IEEE Trans. Ind. Electron.*, vol. 70, no. 1, pp. 975–984, Jan. 2023.
[14] O. M. Barham, M. Mirzaeimoghri, and D. L. DeVoe, "Piezoelectric disc transformer modeling utilizing extended Hamilton's principle," *IEEE Trans. Power Electron.*, vol. 34, no. 7, pp. 6583–6592, Jul. 2019.
[15] M. Ekhtiari, T.-G. Zsurzsan, M. A. Andersen, and Z. Zhang, "Optimum phase shift in the self-oscillating loop for piezoelectric-transformer-based power converters," *IEEE Trans. Power Electron.*, vol. 33, no. 9, pp. 8101–8109, Sep. 2018.
[16] T. Martinez, G. Pillonnet, and F. Costa, "A 15-mV inductor-less start-up converter using a piezoelectric transformer for energy harvesting applications," *IEEE Trans. Power Electron.*, vol. 33, no. 3, pp. 2241–2253, Mar. 2018.
[17] A. Crawford, "Piezoelectric ceramic transformers and filters," *J. Brit. Inst. Radio Eng.*, vol. 21, no. 4, pp. 353–360, 1961.
[18] T. Zaitsu et al., "Piezoelectric transformer operating in thickness extensional vibration and its application to switching converter," in *Proc. Power Electron. Spec. Conf.*, 1994, pp. 585–589.
[19] E. M. Baker, W. Huang, D. Y. Chen, and F. C. Lee, "Radial mode piezoelectric transformer design for fluorescent lamp ballast applications," *IEEE Trans. Power Electron.*, vol. 20, no. 5, pp. 1213–1220, Sep. 2005.
[20] J. Du, J. Hu, and K.-J. Tseng, "High-power, multioutput piezoelectric transformers operating at the thickness-shear vibration mode," *IEEE Trans. Ultrasonics, Ferroelect., Freq. Control*, vol. 51, no. 5, pp. 502–509, May 2004.
[21] R. Prieto, M. Sanz, J. Cobos, P. Alou, O. Garcia, and J. Uceda, "Design considerations of multi-layer piezoelectric transformers," in *Proc. 16th Annu. IEEE Appl. Power Electron. Conf. Expo.*, 2001, pp. 1258–1263.
[22] J. Hu, G. Li, H. Chan, and C. Choy, "An improved method for analyzing the performance of multilayer piezoelectric transformers," in *Proc. IEEE Int. Symp Ultrasonics Symp.*, 1999, pp. 943–946.
[23] H. Tsuchiya and T. Fukami, "Design principles for multilayer piezoelectric transformers," *Ferroelectrics*, vol. 68, no. 1, pp. 225–234, 1986.
[24] G. Ivensky, I. Zafrany, and S. Ben-Yaakov, "Generic operational characteristics of piezoelectric transformers," *IEEE Trans. Power Electron.*, vol. 17, no. 6, pp. 1049–1057, Nov. 2002.
[25] S. Lin, H. Cao, and X. Qiao, "Wireless power transmission based on sandwiched composite piezoelectric transducers in length extensional vibration," *IEEE Trans. Power Electron.*, vol. 31, no. 9, pp. 6134–6143, Sep. 2016.
[26] S. Lin, J. Xu, and H. Cao, "Analysis on the ring-type piezoelectric ceramic transformer in radial vibration," *IEEE Trans. Power Electron.*, vol. 31, no. 7, pp. 5079–5088, Jul. 2016.
[27] S. Lin, J. Hu, and Z. Fu, "Electromechanical characteristics of piezoelectric ceramic transformers in radial vibration composed of concentric piezoelectric ceramic disk and ring," *Smart Mater. Struct.*, vol. 22, no. 4, 2013, Art. no. 045018.
[28] S. Wang, J. Shan, H. Tian, and S. Lin, "The high-power piezoelectric transformer with multiple outputs based on sandwiched piezoelectric transducers," *IEEE Trans. Power Electron.*, vol. 37, no. 8, pp. 8886–8894, Aug. 2022.
[29] S. Wang and S. Lin, "An exact and practical analyzing model for radial vibration of piezoelectric spherical transducers with arbitrary wall thickness," *IEEE Trans. Ultrasonics, Ferroelect., Freq. Control*, vol. 68, no. 3, pp. 760–766, Mar. 2021.
[30] Y. Tang and S. Lin, "Systematic design and experimental realization of a radially cascaded spherical piezoelectric transducer," *J. Acoust. Soc. Amer.*, vol. 154, no. 3, pp. 1838–1849, 2023.
[31] Y. Tang and S. Lin, "Effect of electric impedance on the electromechanical characteristics of tunable spherical piezoelectric transducer," *Ultrasonics*, vol. 136, 2024, Art. no. 107155.
[32] Y. Tang, C. Chen, H. Tian, and S. Lin, "Radial vibration analysis for piezoceramic shell-stacked spherical transducer with thick walls," *Smart Mater. Struct.*, vol. 33, no. 3, 2024, Art. no. 035002.

Yifan Tang was born in Shaanxi Province, China, on August 15, 1991. He received the Ph.D. degree in acoustics from Nanjing University, Nanjing, China, in 2020.

He is currently an Associate Researcher with the School of Physics and Information Technology, Shaanxi Normal University, Xi'an, China. His current research interests include ultrasonic piezoelectric transducers, piezoelectric transformers, acoustic metamaterials, and acoustic artificial devices.

Shuyu Lin was born in Shandong Province, China, on December 22, 1962. He received the Ph.D. degree in physics from the Tokyo Institute of Technology, Tokyo, Japan, in 2002.

He is currently a Professor and the Director of the Applied Acoustics Institute, Shaanxi Normal University, Shaanxi, China. His current research interests include high-power ultrasonics, piezoelectric transducers and resonators, piezoelectric transformers and motors, and different ultrasonic applications. He has authored or coauthored more than 100 papers. His current research fields focus on radially sandwiched piezoelectric ultrasonic transducer, high-power cylindrical ultrasonic transducer, and piezoelectric transformer.

Dr. Lin is currently a Fellow and Administrator of the Acoustical Society of China, and the Director of the Power Ultrasonics Committee of the Acoustical Society of China.